Structure of a NADH-Insensitive Hexameric Citrate Synthase that Resists Acid Inactivation†

Julie A. Francois, Courtney M. Starks, Sasitorn Sivanuntakorn, Hong Jiang, Aaron E. Ransome, Jeong-Won Nam, Charles Z. Constantine, and T. Joseph Kappock*

Department of Chemistry, Washington University, St. Louis, Missouri 63130-4899

Received May 31, 2006; Revised Manuscript Received August 15, 2006

ABSTRACT: *Acetobacter aceti* converts ethanol to acetic acid, and strains highly resistant to both are used to make vinegar. *A. aceti* survives acetic acid exposure by tolerating cytoplasmic acidification, which implies an unusual adaptation of cytoplasmic components to acidic conditions. *A. aceti* citrate synthase (*Aa*CS), a hexameric type II citrate synthase, is required for acetic acid resistance and, therefore, would be expected to function at low pH. Recombinant *Aa*CS has intrinsic acid stability that may be a consequence of strong selective pressure to function at low pH, and unexpectedly high thermal stability for a protein that has evolved to function at ∼30 °C. The crystal structure of *Aa*CS, complexed with oxaloacetate (OAA) and the inhibitor carboxymethyldethia-coenzyme A (CMX), was determined to 1.85 Å resolution using protein purified by a tandem affinity purification procedure. This is the first crystal structure of a "closed" type II CS, and its active site residues interact with OAA and CMX in the same manner observed in the corresponding type I chicken CS·OAA·CMX complex. While *Aa*CS is not regulated by NADH, it retains many of the residues used by *Escherichia coli* CS (*Ec*CS) for NADH binding. The surface of *Aa*CS is abundantly decorated with basic side chains and has many fewer uncompensated acidic charges than *Ec*CS; this constellation of charged residues is stable in varied pH environments and may be advantageous in the *A. aceti* cytoplasm.

Citrate synthase (CS)[1] catalyzes the conversion of oxaloacetate (OAA) and acetyl-coenzyme A (AcCoA) into citrate, coenzyme A, and a proton (Scheme 1). The first half-reaction is an aldol-Claisen condensation requiring the simultaneous protonation of a ketone and deprotonation of an acetyl group. In the rate-limiting second half-reaction, citryl-CoA (CitCoA) is hydrolyzed (*1*). CS is found in two distinct structural types: type I, often represented by pig CS (PCS), and type II, represented by *Escherichia coli* CS (*Ec*CS). Type I CSs are found in most organisms, are dimeric, and have shorter sequences than type II CSs. Type II CSs are found in Gram-negative bacteria, are hexameric, and have an N-terminal β-sheet domain, and some are allosterically inhibited by NADH (*2*, *3*). All characterized CS forms have similar active sites, consistent with conservation of mechanism in a very ancient enzyme.

Progressive CS conformational changes occur as CS binds OAA, which creates the binding pocket for AcCoA, and then in ternary complexes of CS with OAA and AcCoA analogues (*4*−*6*). Crystal structures of CS bound to citrate and coenzyme A (CoA) show additional conformations (*4*, *7*, *8*). The two domains in each CS subunit change relative orientations, but there is no single, easily identifiable "hinge" region. At present, only "open" conformations of type II *Ec*CS have been visualized by X-ray crystallography, including structures with NADH but not substrates bound (*2*, *9*, *10*).

CS is essential for acetic acid resistance in the vinegar-producing bacterium *Acetobacter aceti* (*11*). Like other acetic acid bacteria (AAB), *A. aceti* are Gram-negative, obligately aerobic, acidophilic rods that have been used for millenia to produce vinegar from ethanol (*12*). AAB kill competing

† We gratefully acknowledge support from the Herman Frasch Foundation for Research in Agricultural Chemistry (Grant 531-HF02) and the NSF (CAREER award MCB-0347250). J.A.F. was supported in part by a grant from the U.S. Department of Education (Graduate Assistance in Areas of National Need Grant P200A80221). J.-W.N. was supported by a grant from Monsanto. Mass spectrometry was provided by the Washington University Mass Spectrometry Resource with support from the NIH National Center for Research Resources (P41RR0954).

* To whom correspondence should be addressed. Telephone: (314) 935-8241. Fax: (314) 935-4481. E-mail: kappock@wustl.edu.

[1] Abbreviations: AAB, acetic acid bacteria; *Aa*CS, *A. aceti* CS; *Aa*CS^{dye}, native *Aa*CS purified by dye affinity chromatography; *Aa*CSH6, *Aa*CS with an eight-amino acid C-terminal appendage containing six histidines; *Aa*CS^{intein}, native *Aa*CS cleaved from an intein fusion partner; *aarA*, gene encoding *Aa*CS; AcCoA, acetyl-CoA; α-KG, α-ketoglutarate; amp, ampicillin; CAPS, 3-(cyclohexylamino)propanesulfonic acid; CBD, chitin binding domain; CD, circular dichroism; CHES, 2-(cyclohexylamino)ethanesulfonic acid; CitCoA, citryl-CoA; CMX, carboxymethyldethia-coenzyme A; CoA, coenzyme A; CS, citrate synthase; CV, column volume; Δ*F*, change in fluorescence; dethiaAcCoA, dethiaacetyl-coenzyme A; DTNB, 5,5′-dithiobis(2-nitrobenzoic acid); *Ec*CS, *E. coli* citrate synthase; EDTA, ethylenediaminetetraacetic acid; ESI-MS, electrospray ionization mass spectrometry; gDNA, genomic DNA; *Gg*CS, chicken (*Gallus gallus*) CS; H6, hexahistidine; IDA, iminodiacetic acid−Sepharose; LB, Luria-Bertani medium; M, molecular ion mass; MES, 2-(*N*-morpholino)ethanesulfonic acid; MOPS, 3-(*N*-morpholino)propanesulfonic acid; MW, molecular weight; MWCO, molecular weight cutoff; NCS, noncrystallographic symmetry; OAA, oxaloacetate; ODN, oligodeoxynucleotide; PanK, pantotheinate kinase; PCR, polymerase chain reaction; PCS, pig citrate synthase; *Pf*CS, *Pyrococcus furiosus* CS; PrCoA, *n*-propionyl-CoA; rmsd, root-mean-square deviation; T_m, melting temperature; Tris, tris(hydroxymethyl)aminomethane; YPD, yeast extract peptone dextrose medium.

10.1021/bi061083k CCC: $33.50
Published on Web 10/20/2006

Scheme 1: CS Half-Reactions

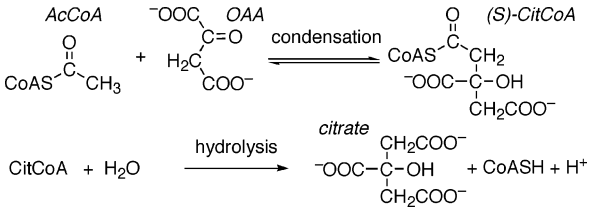

organisms by secreting acetic acid, a membrane-permeable organic acid that acidifies the cytoplasms of susceptible microorganisms, poisoning them and disrupting their proton gradients. During this process, the *A. aceti* cytoplasm also becomes acidic, yet the cells continue growing and oxidizing ethanol even as the cytoplasmic pH drops as low as 3.7 ± 0.2 (*13*). In this respect, *A. aceti* differs from other acidophiles, most of which tolerate only membrane-impermeant mineral acids (e.g., HCl) and avoid cytoplasmic acidification (*14*).

AAB in the genus *Acetobacter* oxidize ethanol, acetic acid, and lactic acid to CO_2, distinguishing them from AAB of the *Gluconobacter* and *Gluconacetobacter* genera, which lack a complete set of citric acid cycle enzymes (*15*) and are used for different industrial purposes (*16*). For example, the complete *Gluconobacter suboxydans* genome lacks recognizable genes for three citric acid cycle enzymes (*17*). The use of a complete citric acid cycle to oxidize excess acetic acid might help explain the greater acid tolerance of *Acetobacter* species relative to other AAB genera (*18*). *A. aceti* cultures grown at high acetic acid and ethanol levels require vigorous aeration (*19*, *20*), which is also consistent with cytoplasmic acetate disposal using the citric acid cycle. Expressing either of the first two citric acid cycle enzymes (CS or aconitase) improves the acetic acid resistance of AAB (*11*, *21*).

Citrate synthase from industrial *A. aceti* strain 1023 (*Aa*CS) is a type II CS that lacks several amino acid residues implicated in NADH binding (*9*). In facultative anaerobes, NADH allosterically inhibits CS, downregulating the citric acid cycle during anaerobic growth. Because *A. aceti* is a strict aerobe, it may not be surprising that *Aa*CS lacks a NADH binding site. Since *Aa*CS is required for acetic acid resistance in *A. aceti*, selection against inhibition by NADH [which binds *Ec*CS more tightly at low pH (*22*)] may have been a more important factor.

With an acidic cytoplasm that exerts strong selective pressure against acid-mediated inactivation, *A. aceti* should be a rich source of acid-adapted proteins. Many familiar acid-stable proteins from other organisms are found in the periplasm (e.g., rusticyanin) or are secreted enzymes (e.g., pepsin); however, secreted proteins are not subject to the same selective pressures as cytoplasmic enzymes, which are regulated and substrate-specific and function in a metabolic context (*23*). In contrast, all cytoplasmic enzymes in *A. aceti* function at low pH. Comparisons of the biophysical features of multiple cytoplasmic proteins from *A. aceti* should reveal if acid resistance is achieved through common, recognizable strategies. The *A. aceti* proteome may also represent a library of enzymes that are useful for acidic bioprocesses.

Here we describe the purification, biochemical characterization, and determination of the structure of *Aa*CS. As predicted, *Aa*CS resists acid-mediated inactivation and is not affected by NADH. Surprisingly, *Aa*CS is also thermostable,

Chart 1: AcCoA and Analogues

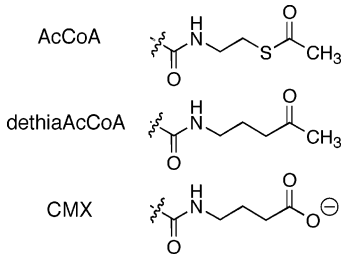

which suggests that acid- and temperature-stabilizing features in this protein might be related. The crystal structure presented here, of *Aa*CS in complex with OAA and an AcCoA analogue, is the first of a "closed" type II CS.

EXPERIMENTAL PROCEDURES

Materials, general analytical procedures, and procedures for determining extinction coefficients, assessing OAA decomposition, and determining OAA binding constants are provided as Supporting Information.

Synthesis of AcCoA Analogues. Dethiaacetyl-coenzyme A (dethiaAcCoA) and carboxymethyldethia-coenzyme A (CMX, Chart 1) were synthesized by using the procedure of Drueckhammer and co-workers (*24*) updated to use pantothenate kinase (PanK) to phosphorylate *S*-propyl thiopantothenate (*25*). Modifications to these procedures, and analytical data for the products, are given as Supporting Information.

Bacterial Strains and Growth Conditions. Routine cloning procedures were performed with *E. coli* DH5α. *E. coli* W620 (*thi-1 pyrD36 gltA6 galK30 rpsL129*), obtained from the *E. coli* Genetic Stock Center, was used to test for complementation of the *gltA* mutation (*26*, *27*) and was grown on M9 minimal medium supplemented with 0.02 mM thiamine, 0.1 mg/mL ampicillin (amp), and when appropriate 3 mM L-glutamate. *A. aceti* strain 1023 was grown in YPD supplemented with 2.5% (v/v) ethanol at 30 °C.

DNA Manipulations. Genomic DNA (gDNA) from *A. aceti* 1023 was isolated using a Genomic-tip 20/G device (Qiagen). gDNA (10 μg) was digested for 2.5 h at 37 °C with BamHI (18 units) and then reisolated using a QIAquick spin column (Qiagen). In a final volume of 50 μL, BamHI-digested gDNA (0.3 μg) was ligated to an adaptor (30 pmol) created by annealing oligonucleotides (ODNs) 532 and 554 (Supporting Information, Table S1), which form a partial duplex at their 3′ ends.

The *A. aceti* 1023 AarA gene was amplified by PCR using ODNs 413 and 416, and 3 ng of adaptor-ligated *A. aceti* strain 1023 gDNA as a template. The PCR product was digested and ligated into pET23a (Novagen) cut with NdeI and EcoRI to create plasmid pJK136. DNA sequencing revealed three single-base differences from the published sequence (GenBank accession number M34830), leading to two changes in the deduced amino acid sequence: codon 85 is GCC (Ala), not GAC (Asp), and codon 106 is GCG (Ala), not GTG (Val). There is also a silent difference in codon 50 (Phe). Two independently amplified PCR products containing AarA were found to have the same two differences in their DNA sequences. Our *Aa*CS sequence has been deposited in GenBank as accession number DQ631551.

QuikChange (Stratagene) mutagenesis of pJK136 with ODNs 865 and 866 gave plasmid pJK225, which encodes AarA with the LEHHHHHH octapeptide added to the C-terminus (*Aa*CSH6). The NdeI−EcoRI fragment from pJK136 was ligated into pTWIN1 to give plasmid pJK226. Mutagenesis of pJK226 with ODNs 867 and 868 gave plasmid pJK227, which changes the *Aa*CS TAA stop codon to TGC (Cys) and places the coding region for the C-terminal *Mxe* GyrA intein in frame. Mutagenesis with ODNs 884 and 885 gave plasmid pJK240, which adds a hexahistidine (H6) tag to the C-terminus of the plasmid-encoded chitin binding domain (CBD), to produce the *Aa*CS−intein−CBD-H6 fusion protein.

*Overexpression and Purification of AaCS Forms. Aa*CS^{dye} was produced in *E. coli* B834(DE3) or BL21(DE3) transformed with plasmid pJK136 and purified using a dye ligand affinity column as described in the Supporting Information (Table S2). *Aa*CSH6 was produced in *E. coli* BL21(DE3) transformed with pJK225 and purified by ammonium sulfate fractionation and Ni^{2+} affinity chromatography as described in the Supporting Information.

*Aa*CS^{intein} was produced in *E. coli* BL21(DE3) or C41-(DE3) transformed with pJK240. Protein expression was carried out in a 1 L culture of LB/amp in a 2.8 L Fernbach flask induced with 0.2 mM IPTG for 16−18 h at 15 °C. Cells from a 1 L growth were resuspended in buffer H [20 mM Tris (pH 8.0) and 100 mM KCl] at 5 mL/g of cells and then sonicated and treated with streptomycin as described for *Aa*CS^{dye}. The supernatant was applied to an iminodiacetic acid−Sepharose (IDA)−Ni^{2+} column (2.5 cm × 3.5 cm), which was then washed with 3 column volumes (CV) of buffer H containing 20 mM imidazole. The IDA−Ni^{2+} column was developed with a linear gradient from 20 to 500 mM imidazole (50 × 50 mL, 7 CV) in buffer H.[2] Fractions containing protein were concentrated, buffer exchanged to reduce the imidazole concentration to 5−10 mM, and loaded onto a chitin column (2.5 cm × 6 cm).[3] The chitin column was then washed with 3 CV of buffer H and flushed with 3 CV of buffer HD (buffer H with 50 mM DTT). After 3 days, the liberated *Aa*CS^{intein} was eluted using buffer HD. Fractions containing *Aa*CS^{intein} were pooled and concentrated. At this stage, the protein was generally frozen in single-use aliquots and stored at −80 °C. *Aa*CS ^{intein} used for crystallization was further purified by gel filtration on a Superdex 200 column (2.5 cm × 60 cm, Amersham) in buffer H. Purified enzyme was then concentrated, exchanged into 5 mM Tris (pH 8.0) and 10 mM NaCl, and stored in aliquots at −80 °C.

AaCS Oligomerization States. Analytical gel filtration was carried out at 5 °C on a Tosoh TSK-GEL G2000SWXL column (0.78 cm × 30 cm) in 50 mM sodium phosphate (pH 7.0) and 150 mM NaCl. The column was calibrated with thyroglobulin (670 kDa), bovine γ-globulin (159 kDa), chicken ovalbumin (44 kDa), equine myoglobin (17 kDa), vitamin B12 (1.3 kDa), and acetone (0.06 kDa). *Aa*CS^{dye} or *Aa*CSH6 (20 μg in 20 μL; initial subunit concentration of 21 μM) was loaded onto the column and eluted at 0.4 mL/min in the equilibration buffer. Molecular sizes of unknown protein species were determined using the log MW versus K_{SEC} calibration method (*28*).

Enzyme Assays. Enzyme activities were determined by two continuous assay methods: (A) using 5,5′-dithiobis(2-nitrobenzoic acid) (DTNB) in a coupled assay that detects formation of CoA thiol at 412 nm (*29*, *30*) or (B) monitoring cleavage of the thioester in AcCoA at 233 nm (*31*). All assays were initiated by the addition of CS to an otherwise complete 0.5 mL reaction mixture equilibrated at 25 °C for 3 min. One unit of activity is defined as 1 μmol of product formed per minute at 25 °C. Potential inhibitors and alternative substrates were tested as described in the Supporting Information.

Assay A reaction mixtures contained (final concentrations) 50 mM Tris-HCl (pH 8.0), 2 mM EDTA, 100 mM KCl, 0.4 mM OAA, 0.3 mM DTNB, 0.15 mM AcCoA, and 0.04−0.1 μg of CS. The optimal KCl concentration was determined over the range of 0−0.5 M. Kinetic constants were determined by varying the OAA concentration from 1 to 500 μM or the AcCoA concentration from 1 to 750 μM, holding all other concentrations fixed as in the standard activity assay.

Assay B reaction mixtures contained (final concentrations) 50 mM potassium phosphate (pH 8.0), 100 mM KCl, 0.4 mM OAA, 0.15 mM AcCoA, and 0.07−0.2 μg of CS. A 0.5 cm path length quartz cuvette was used. Kinetic constants were determined by varying the OAA concentration from 1 to 750 μM or the AcCoA concentration from 5 to 750 μM, holding all other concentrations fixed as in the standard activity assay. Substrate saturation curves were fit to the Michaelis−Menten equation.

pH−rate profiles were constructed using assay B from pH 3.5 to 8.5 and assay A from pH 7.0 to 10.5 with 50 mM buffer and 100 mM KCl. Buffers were potassium phosphate (pH 3.5−8.0), CHES (pH 8.5−9.5), and CAPS (pH 10.0−10.5). Kaliedagraph (Abelbeck Software) was used for nonlinear least-squares fits of y (either k_{cat} or k_{cat}/K_m, obtained from fits to the Michaelis−Menten equation) to eq 1, yielding c, the pH-independent form of the parameter y, and K_a values.

$$\log y = \log\left(\frac{c}{1 + H/K_{a1} + K_{a2}/H}\right) \qquad (1)$$

Acid Stability Assays. Inactivation of CS was used as a reporter for protein unfolding. *Aa*CS^{dye} or *Aa*CSH6 was incubated at 0.7−1.4 μM (subunit concentrations, 0.03−0.07 mg/mL) at 30 °C in 50 mM potassium phosphate and 100 mM KCl at pH 3.5−7.0. Aliquots (0.12−2.4 μg) were withdrawn over time and added to an otherwise complete activity assay mixture equilibrated for 3 min at 25 °C. Meaningful zero-time points are not obtained in these experiments. All inactivation rates were determined by fits of single-exponential decays to the activity remaining versus time plot. Similar experiments were performed using incubations in different buffers (acetate, citrate, MES, or MOPS) at higher protein concentrations (5 μM subunits, 0.24 mg/mL), or with PCS instead of *Aa*CS.

Crystal Structure Determination and Analysis. All crystallization experiments were carried out at room temperature using the hanging drop vapor diffusion method. Ternary complexes were prepared by combining *Aa*CS^{intein} (6.5 μM subunit concentration), OAA (5 mM), and either dethia-AcCoA or CMX (15 μM) prior to buffer exchange and

[2] The IDA−Ni^{2+} column can also be eluted in a single step with buffer H and 250 mM imidazole.

[3] Fractions in 250 mM imidazole can be loaded directly onto the chitin column.

concentration as described above. Crystals were screened for diffraction using a Rigaku R-Axis IV image plate detector and a graphite-monochromated Cu Kα X-ray beam from a Rigaku RU200 generator operated at 5 keV.

Crystals of the *Aa*CS·OAA·CMX complex were grown in 2.1 M ammonium sulfate, 150 mM sodium potassium tartrate, and 35 mM sodium citrate (pH 5.4). Prior to data collection, crystals were briefly dunked in crystallization solution with 25% (v/v) glycerol and then frozen in liquid nitrogen. A data set was collected from a single crystal at Advanced Light Source beamline 4.2.2. Data were indexed, integrated, and scaled using d*TREK (*32*) and then converted to structure factor amplitudes using the Truncate (*33*) program in CCP4 (*34*). The crystal was indexed with a primitive orthorhombic lattice, and examination of systematic absences allowed the $P2_12_12_1$ space group to be assigned. Placing six 47 kDa monomers in the asymmetric unit would result in a solvent content of 57%, suggesting that the asymmetric unit likely contained a complete hexamer.

A search model for molecular replacement was generated starting with the *Pyrococcus furiosus* citrate synthase (*Pf*CS) dimer (PDB entry 1aj8) (*7*). This structure was aligned with two subunits of the hexameric *Ec*CS structure (PDB entry 1k3p) (*2*), and regions that varied most between the two structures were removed. The search model then contained (*Pf*CS numbering) residues 15−106, 124−167, 174−218, and 311−350 in each monomer. Side chains were then pruned to minimal conserved shapes using SEAMAN (*35*). For example, if the *Aa*CS sequence had a Val in a position occupied by an Ile in 1aj8, the position would be mutated to a Val in the corresponding conformation.

The structure of *Aa*CS was determined by molecular replacement using MOLREP (*36*), specifying that three copies of the dimeric starting model should be located in the asymmetric unit. The top solution had good crystal packing and a hexameric arrangement resembling that of *Ec*CS. Rigid body refinement was then carried out in CNS (*37*), using data to 3 Å and allowing all protein segments to move independently. The resulting model had an *R*-factor of 51.0% (R_{free} = 51.2%); a 2 Å $2F_o - F_c$ electron density map calculated with phases from this model revealed clear density for side chains that were not modeled, as well as for large protein segments that were not modeled.

Several rounds of manual building of chain A in O (*38*) and simulated annealing in CNS with data to 2 Å using noncrystallographic symmetry (NCS) to generate the hexamer were then carried out, resulting in an *R*-factor of 31.1% (R_{free} = 33.6%). In subsequent rounds, each subunit of the hexamer was refined and manually adjusted without NCS restraints. OAA and CMX were then modeled into clear, unambiguous electron density in each active site. Additional rounds of water addition, manual rebuilding, and positional and *B*-factor refinement using CNS and REFMAC (*39*) were carried out. Several solvent peaks in the electron density map with tetrahedral or nearly tetrahedral geometry were modeled as sulfate ions.

Calculations of root-mean-square differences (rmsd) between protein models were carried out in LSQMAN (*40*); calculations of buried surface areas were conducted in Chimera (*41*). Figures were rendered using PyMOL (*42*), Molscript (*43*), and Raster3D (*44*). Electrostatic calculations were performed using PDB2PQR (*45*) and APBS (*46*).

RESULTS

Recombinant AaCS Expression and Characterization. The *A. aceti* strain 1023 *aarA* gene encoding *Aa*CS was cloned into several T7 expression vectors. The inferred protein sequence differed from previous reports at two amino acids: amino acid 85 being Ala, not Asp, and amino acid 106 being Ala, not Val. Plasmid pJK136, encoding *Aa*CS, restored prototrophy to *gltA* strain W620.

Recombinant *Aa*CS (*Aa*CS^{dye}) with a specific activity of 112 ± 11 units/mg was purified with a dye−ligand affinity purification step with Blue Sepharose resin (Supporting Information, Table S2 and Figure S1A), a technique selective for (acyl) CoA binding proteins (*47*). Repeated attempts to adsorb *Aa*CS onto ion-exchange columns in low-ionic strength buffer solutions at pH 6.5−9.0 failed or gave inconsistent results. Slightly basic conditions allowed removal of most *E. coli* proteins with a short DE-52 column; this step improved the performance of the subsequent Blue Sepharose chromatography. Pure *Aa*CS^{dye} can be stored at pH 8.0 for up to 1 week at 4 °C without a significant loss of activity.

Adding a C-terminal affinity tag to the AarA gene yielded *Aa*CSH6, a protein that is easier to purify and has the same specific activity (111 ± 12 units/mg). A third construct was generated to produce *Aa*CS fused to an intein tag, a chitin binding domain (CBD), and a hexahistidine tag. After metal and chitin affinity chromatography steps, native *Aa*CS (*Aa*CS^{intein}) was released by thiol-mediated self-cleavage of the intein tag, along with the CBD and hexahistidine tag. The resulting enzyme has a specific activity (123 units/mg) similar to those produced with the other two constructs (Supporting Information, Table S3 and Figure S1).

Electrospray ionization mass spectrometry (ESI-MS) showed that each pure protein lacked a Met residue, presumably Met1: for *Aa*CS^{dye} and *Aa*CS^{intein}, an ion at *m*/*z* 47 994 was observed (expected 47 994.4), and for *Aa*CSH6, an ion at *m*/*z* 49 057 was observed (expected 49 059.5). Each mass spectrum also exhibited an intense ion signal at *m*/*z* [M − Met − 60]. This uncommon but precedented fragmentation is consistent with loss of either a guanidinium ion or a neutral guanidine from an arginine residue during the MS experiment (*48*, *49*). The relative intensity of the [M − Met − 60] peak increases with the capillary potential but is unaffected by the accelerating potential.

Molecular sizes were determined by analytical size exclusion chromatography in the absence of both KCl and NADH, each of which promotes hexamer formation in the NADH-sensitive *Ec*CS (*50*, *51*). Unliganded *Aa*CSH6 had an apparent molecular mass of 305 kDa, corresponding to a hexamer of 49 kDa subunits. Minor peaks consistent with larger aggregates and with dimers (∼70 kDa)[4] were also observed (the dimer peak area was ≤7% of the hexamer peak area). This is in contrast with *Ec*CS, which at comparable subunit concentrations and in the absence of NADH favors the dimer over the hexamer (*50*).

Enzyme Characterization. Kinetic constants for the three *Aa*CS constructs are similar (Table 1), and except where

[4] While a 70 kDa peak has an apparent molecular mass that is smaller than what is expected for a dimer, it is unlikely to be a monomer given the extensive interactions between monomers observed in all known CS structures.

Table 1: Kinetic and Binding Constants for *Aa*CS Purified by Different Methods

	*Aa*CS^{dye}	*Aa*CSH6	*Aa*CS^{intein}
K_m^{OAA} (μM)[a]	6.2 ± 2[b]	5.1 ± 0.3	17 ± 3
K_m^{AcCoA} (μM)[a]	36 ± 7	29 ± 3	37 ± 6
k_{cat} (min^{-1})[a]	6000 ± 300	5400 ± 140	5700 ± 240
K_m^{CitCoA} (μM)[a]	16 ± 3	20 ± 2	18 ± 3
k_{cat}^{CitCoA} (min^{-1})[a]	5400 ± 400	6200 ± 370	6100 ± 400
pK_{a1}			
k_{cat}/K_m(sat OAA)	5.28 ± 0.06	5.7 ± 0.1	5.1 ± 0.1
k_{cat}/K_m(sat AcCoA)	nd[c]	nd[c]	5.1 ± 0.2
k_{cat}(sat OAA)	5.16 ± 0.08	5.20 ± 0.08	5.3 ± 0.1
k_{cat}(sat AcCoA)	nd[c]	nd[c]	5.2 ± 0.1
pK_{a2}			
k_{cat}/K_m(sat OAA)	9.16 ± 0.08	9.2 ± 0.2	9.4 ± 0.1
k_{cat}/K_m(sat AcCoA)	nd[c]	nd[c]	8.9 ± 0.2
k_{cat}(sat OAA)	10.1 ± 0.2	10.3 ± 0.2	10.3 ± 0.2
k_{cat}(sat AcCoA)	nd[c]	nd[c]	9.6 ± 0.2
K_d^{OAA} (μM), pH 8.0	21.1 ± 0.9	22.8 ± 0.7	22.9 ± 0.6
K_d^{OAA} (μM), pH 4.7	16.0 ± 0.7	18.5 ± 0.8	18.9 ± 0.7

[a] Measured at pH 8.0 and 25 °C using assay A (DTNB-coupled). [b] The OAA K_m vs pH fit (Supporting Information, Figure S8) gives 14 μM at pH 8, with a pK_{a1} of 4.3 ± 0.4 and a pK_{a2} of 8.9 ± 0.3. [c] Not determined.

noted, all further enzymatic characterization refers to *Aa*CS-^{dye}. K_m values for OAA and AcCoA are closer to the K_m values for *Gluconacetobacter europaeus* CS (20 and 51 μM) (*52*) than to those of *Ec*CS (26 and 120 μM) (*10*) or PCS (5.9 and 5.1 μM) (*53*). These CSs had comparable k_{cat} values (14 000, 4900, and 10 000 min^{-1}, respectively) in slight variants of assay A. Potential inhibitors and alternative substrates were examined, as described in the Supporting Information (Table S4 and Figure S2).

Sequence alignments indicate that *Aa*CS is a type II CS but lacks an intact allosteric site for NADH (*9*). *Ec*CS is strongly inhibited by NADH (*54*), which binds tightly (K_d ~ 2 μM) even when key active site residues are mutated (*55*). KCl weakens NADH-mediated *Ec*CS inhibition and has other stimulatory effects (*54*, *56*). KCl was not required for *Aa*CS activity, but increasing its concentration from 0 to 0.1 M increased the specific activity by 10−20%. Inhibition of *Aa*CS by NADH was examined at up to 0.5 mM NADH with the KCl concentration varied from 0 to 0.4 M. The strongest apparent NADH inhibition was observed at 0.1 M KCl. The strength of NADH inhibition under these conditions was then examined using steady-state kinetics (Supporting Information, Figure S3). NADH is a weak *Aa*CS inhibitor, with a noncompetitive inhibition pattern versus AcCoA at saturating OAA concentrations (K_{ii} = 69 mM; K_{is} = 95 mM).

*Aa*CS contains four Trp residues, which fluoresce with an emission λ_{max} of 339 nm (excitation at 295 nm). The fluorescence was quenched 25−30% by the addition of OAA to *Aa*CS^{dye} or *Aa*CSH6 (Supporting Information, Figure S4). *Aa*CS and *Aa*CSH6 had the same emission λ_{max}, and each exhibited a small red shift (3 nm) on OAA binding (emission λ_{max} = 342 nm). Similar changes in fluorescence emission were observed for *Thermoplasma acidophilum* CS (*57*), in which Trp348, analogous to *Aa*CS Trp400, is the primary emitter (*58*). Its fluorescence is quenched by OAA binding nearby. Fluorescence changes were used to measure the K_d for OAA at pH 4.7 or 8.0 (Table 1; Supporting Information, Figure S5), under conditions that minimize photodecomposition (<4% of the observed ΔF). Accounting for photodecomposition had no effect on K_ds. Spontaneous OAA decomposition ($t_{1/2}$ = 13 h at 25 °C and pH 3.5−9.0) was not significant (<2%) in the time required to determine K_d values (Supporting Information, Figures S6 and S7).

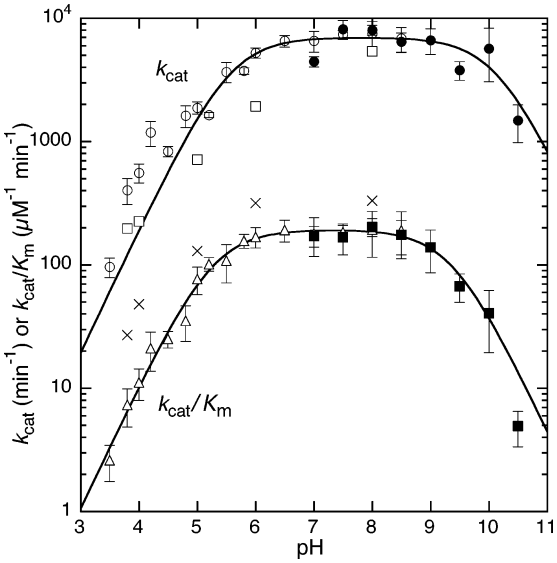

FIGURE 1: pH−rate profiles for *Aa*CS^{dye} using parameters from AcCoA saturation plots for k_{cat} or k_{cat}/K_m vs pH. Solid lines are fits to eq 1. Each point represents a parameter from a fit to the Michaelis−Menten equation of a velocity vs AcCoA concentration plot, performed using assay A [k_{cat} (●) and k_{cat}/K_m (■)] or assay B [k_{cat} (○) and k_{cat}/K_m (△)]. CitCoA k_{cat} (□) and k_{cat}/K_m (×) are also shown. OAA was omitted from the assays with CitCoA. Error bars represent the uncertainty (k_{cat}) or the root-mean-square (rms) uncertainty (k_{cat}/K_m) of the parameter(s) fit. Only the AcCoA data between pH 4.0 and 9.8 were obtained under conditions clearly saturating in OAA, but all data points were included in the fit.

pH−Rate Profiles. A pH−rate profile was assembled to learn if *Aa*CS is broadly active over a range of pH or if it is optimized for activity at low pH. Extinction coefficients at 233 nm needed in the pH range of 3.5−8.5 were determined for OAA (0.73 ± 0.06 mM^{-1} cm^{-1}), AcCoA (7.6 ± 0.6 mM^{-1} cm^{-1}), citrate (~0.01 mM^{-1} cm^{-1}), and CoA (1.8 ± 0.1 mM^{-1} cm^{-1} at pH ≤8.5). At pH ≤8.5 under our experimental conditions, $\Delta\epsilon_{233}$ = 6.5 ± 0.8 mM^{-1} cm^{-1}, somewhat higher than the published value of 5.4 mM^{-1} cm^{-1} (*59*). For a two-substrate enzyme with an ordered substrate binding mechanism, initial rates for a pH−rate profile are determined at saturating levels of the first substrate (*60*). The preferred order of substrate binding by CS is OAA and then AcCoA, with accompanying protein conformational changes (*57*, *61*, *62*). OAA K_m values were determined from pH 3.5 to 10.5 (Supporting Information, Figure S8). In the experiments used for AcCoA, pH−rate determinations, OAA was unambiguously saturating (≥8K_m) in the pH range of 3.8−9.8.

Kinetic constants from AcCoA saturation curves, measured using both activity assays, were used to construct bell-shaped pH−rate profiles for *Aa*CS^{dye} (Figure 1; more profiles are given in the Supporting Information, Figures S9−S11). The pK_a values obtained for all *Aa*CS forms were similar to each other and those for PCS (6.5 and 10.1) (*31*). The k_{cat} and k_{cat}/K_m plots have the same value for pK_{a1}, indicating this inhibitory protonation occurs on *Aa*CS complexed to OAA. Possible candidates for pK_{a1} include Asp371 (*Ec*CS Asp362 and PCS Asp375), which helps bind and enolize AcCoA (*63*, *64*), and the OAA carboxylates, which are not involved in

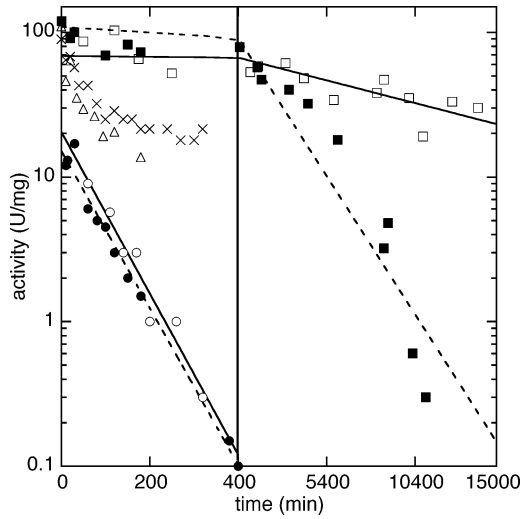

FIGURE 2: Semilogarithmic plot showing acid stability assays at 30 °C. At the indicated times, aliquots were withdrawn from the low-pH enzyme incubation solution and used to initiate an otherwise standard activity assay A. Inactivations of *Aa*CS^{dye} were carried out at pH 3.5 and 0.033 mg/mL (○), pH 3.5 and 0.24 mg/mL (△), and pH 4.0 and 0.033 mg/mL (□). Inactivations of *Aa*CSH6 were carried out at pH 3.5 and 0.071 mg/mL (●), pH 3.5 and 0.24 mg/mL (×), and pH 4.0 and 0.071 mg/mL (■). Fits shown are single-exponential fits to data obtained at $t > 0$ [(—) *Aa*CS^{dye} and (- - -) *Aa*CSH6]. The higher-concentration incubations at pH 3.5 show at least two phases. The time axis is compressed 25-fold to the right of the vertical line at 400 min.

catalysis. The pK_{a2} values are slightly higher in the k_{cat} pH−rate plots, representing ionizations in the Michaelis complex (*Aa*CS·OAA·AcCoA). Candidates include one of the active site histidines [His272 (PCS His274), involved in AcCoA enolization, or His313 (PCS His320), involved in polarizing the OAA ketone] with pK_as shifted above their normal value (∼6.5) by OAA-mediated stabilization of the protonated form. One or more arginines (314, 364, and 414′) that bind AcCoA phosphates might also be responsible. Caution in the interpretation of pK_a values is warranted: CS adopts multiple conformations, including during the catalytic cycle (*65*), and mutagenesis studies indicate that key active site residues participate in both reactions performed by CS (*66*).

Acid Resistance. Kinetic assays measuring the loss of *Aa*CS activity upon incubation at low pH were performed at the typical growth temperature of *A. aceti* over the entire known cytoplasmic pH range (Figure 2). Between pH 3.5 and 6.0, the inactivation rate for *Aa*CSH6 was suitable for accurate rate determinations; a narrower range was useful for *Aa*CS^{dye}, which was too stable at pH >4.0. (The six additional His residues present in *Aa*CSH6 are positively charged at pH 3.5, a potentially destabilizing factor not present in *Aa*CS^{dye}.) At low enzyme concentrations, reasonable fits to single-exponential decays were obtained (Table 2). The inactivation rates for both *Aa*CS^{dye} and *Aa*CSH6 increased sharply at pH <4, but both were substantially more stable than PCS (at pH 3.5, $t_{1/2}$ = 54, 58, and 1 min, respectively). At pH 3.5, the apparent initial activity was lower than expected, suggesting that a partial inactivation occurred in the dead time of this experiment, ∼1 min. Incubations performed at higher *Aa*CS^{dye} or *Aa*CSH6 concentrations yielded slower inactivation at pH 3.5, by a non-single-exponential process.

Table 2: CS Inactivation Rate Constants and T_ms

	inactivation rate (min^{-1})[a]			T_m (°C)	
pH	*Aa*CS	*Aa*CSH6	PCS	*Aa*CS	*Aa*CSH6
3.5	0.013(1)[b]	0.012(2)	4.25(5)	58.3	58.4
3.8	0.00007(1)	0.0012(7)	nd[c]	nd[c]	nd[c]
4.0	0.00007(1)	0.0004(1)	0.014(2)	69.5	69.1
5.0	≤0.00002	0.00005(1)	nd[c]	nd[c]	nd[c]
6.0	≤0.00002	≤0.00002	nd[c]	72.2	70.2
8.0	nd[c]	nd[c]	nd[c]	70.5	70.0

[a] The acid stability assay was used to measure loss of CS activity in incubations at low pH and 30 °C. Rates and uncertainties were obtained from single-parameter fits of all $t > 0$ data to a first-order decay. Initial amplitudes were fixed at values obtained from separate two-parameter fits. [b] Uncertainties in the last significant figure are given in parentheses. [c] Not determined.

CD spectra for *Aa*CS at various pH values were consistent with a largely helical protein (Supporting Information, Figure S12A). CD was used to monitor the irreversible thermal denaturation of *Aa*CS (Supporting Information, Figure S12B) and determine apparent T_m values (Table 2). Thermal unfolding of *Aa*CS generally caused visible protein precipitation; however, the enzyme did not precipitate at pH 3.5, even after overnight incubation at 5 °C. When heated, *Aa*CS partially unfolded at pH 3.5, yielding an altered CD spectrum (Supporting Information, Figure S12A) consistent with a more β-rich structure (*67*). CD denaturation profiles indicate that at pH ≥4.0 *Aa*CS is substantially (∼20 °C) more thermostable than PCS, which unfolds irreversibly with a T_m of 48 °C at pH 7.5 (*68*−*70*). The thermal denaturation profile of *Ec*CS is biphasic with an onset at ∼50 °C (*71*) and, therefore, is difficult to compare with the monophasic *Aa*CS profiles.

Crystal Structure of AaCS. Crystallization of *Aa*CS was initially attempted using *Aa*CS^{dye} and *Aa*CSH6, the second of which gave more promising crystals. *Aa*CSH6 crystallized under a variety of different PEG conditions, forming small rod-shaped crystals or clusters of very thin crystals. Cocrystallization of *Aa*CSH6 with enzyme substrates, substrate analogues (dethiaAcCoA or CMX), or products did not improve crystal quality (J.-W. Nam and W. Wikoff, unpublished observations). The *Aa*CS^{intein} protein, however, crystallized readily as a complex with OAA and CMX.

The structure of *Aa*CS complexed with OAA and CMX was determined by molecular replacement using the dimeric *Pf*CS from the hyperthermophile *P. furiosus* as a search model. The initial molecular replacement solution consisted of a trimer of dimers within the asymmetric unit, representing the enzymatically active hexamer. The initial $2F_o - F_c$ electron density maps allowed unambiguous tracing of most of the polypeptide chain. Several rounds of refinement and manual rebuilding resulted in a model containing a nearly complete polypeptide chain for each of the six monomers; maps calculated with phases from this model revealed clear electron density for OAA and CMX, which were then built into each active site. Electron density for one active site is shown in Figure S13 of the Supporting Information. Surface loops including residues 1−10 (all chains) and 155−163 (chains A, D, and F) are disordered and are not modeled. The current crystallographic model has been refined to an *R*-factor of 19.5% (R_{free} = 23.1%). Refinement data and statistics are given in Table 3. Coordinates and structure

Table 3: Crystallographic Data and Refinement Statistics

PDB entry	2h12
space group	$P2_12_12_1$
cell dimensions	$a = 170.7$ Å, $b = 125.7$ Å, $c = 150.6$ Å, $\alpha = \beta = \gamma = 90°$
resolution (highest shell)	40−1.85 Å (1.92−1.85 Å)
no. of reflections (total/unique)	1959318/274629
completeness (highest shell)	100.0% (99.9%)
$\langle I/\sigma \rangle$ (highest shell)	8.6 (2.6)
R_{sym}[a] (highest shell)	9.0% (49.1%)
R_{cryst}[b]/R_{free}[c]	19.5%/23.1%
no. of protein atoms	19727
no. of water molecules	3229
no. of ligand ions	12
no. of sulfate ions	41
rmsd for bond lengths	0.006 Å
rmsd for bond angles	1.48°
average *B*-factor	23.0 Å^2

[a] $R_{sym} = \sum|I_h - \langle I_h \rangle|/\sum I_h$, where $\langle I_h \rangle$ is the average intensity over symmetry. [b] $R_{cryst} = \sum|F_o - \langle F_c \rangle|/\sum F_o$, where the summation is over the data used for refinement. [c] R_{free} is defined in the same way as R_{cryst} but was calculated using the 5% of the data excluded from refinement.

factors have been deposited in the RCSB Protein Data Bank (PDB) as entry 2h12.

The overall shape of the *Aa*CS hexamer is that of a left-handed turbine or thick propeller, approximately 125 Å in diameter and 80 Å tall. The *Aa*CS hexamer has the same trimer-of-dimers arrangement as *Ec*CS. The three dimeric units are tilted ~30° from the molecular 3-fold axis, and the clefts between the dimers are occupied by seven to nine sulfate ions. Each dimer interface is extensive, burying ~5900 Å^2 of solvent-accessible surface per monomer, while interdimer contacts are localized along the central water-filled cavity and bury ~900 Å^2 per monomer. Like that of *Ec*CS, the *Aa*CS central cavity is lined with basic residues, including (*Ec*CS numbering in parentheses) Arg126 (Arg119), Arg133 (Arg125), and Arg134 (Arg126). The crystal structures of *Aa*CS and *Ec*CS (PDB entry 1owb) hexamers have 51 and 50% polar surface area, respectively. This fraction is the same in the dimers of chicken CS (*Gg*CS, 50% in PDB entry 1csi) and PCS (52% in PDB entry 4cts). This contrasts with another acid-stable enzyme, *A. aceti* PurE, which has much less polar surface area than other PurE forms (*72*). The most striking difference between the *Ec*CS and *Aa*CS surfaces is the large proportion of basic residues on the *Aa*CS surface (Figure 3). Comparisons of several structural features between *Aa*CS and *Ec*CS are given in Table 4.

The monomer structure of CS is very similar in all the type I and type II CSs with known structures, including the *Aa*CS structure described here (Figure 4). *Aa*CS consists of 16 α-helices, analogous to those in other archaeal and bacterial enzymes. Like *Ec*CS, *Aa*CS also has an N-terminal region that folds into a β-sheet with residues from the adjacent monomer and a C-terminal loop that extends along the surface of the adjacent monomer. The individual monomers of *Aa*CS are nearly identical to one another, with rmsd between chains of 0.24−0.28 Å over 417 Cα atoms. The most variable regions among monomers are surface loops near residues 340 and 412, as well as helical regions comprising residues 278−307 and 332−336.

Each *Aa*CS monomer contains one active site, which consists of an OAA binding site in the interior of the protein

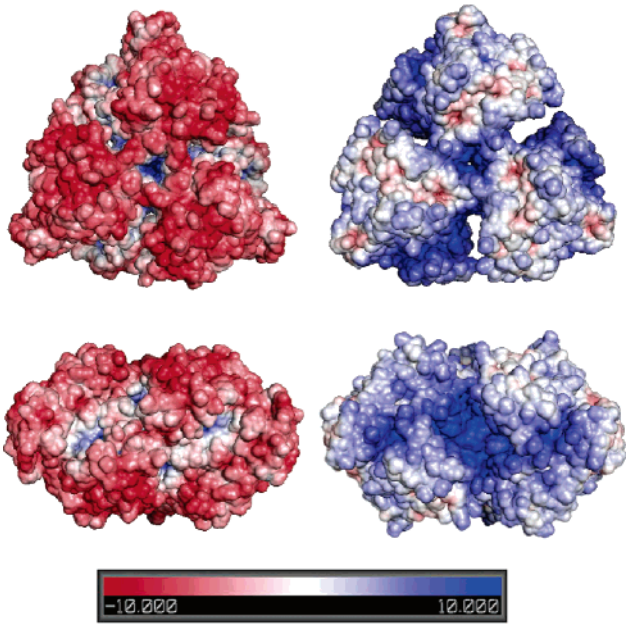

FIGURE 3: Electrostatic rendering of the solvent-accessible surface of *Ec*CS (left) and *Aa*CS (right). Top and side views are given for each hexamer. Computed at pH 7 with red (−10 kT/e) and blue (10 kT/e).

at the end of an ~20 Å CoA binding tunnel. Several crystal structures are available for type I CS bound to CoA derivatives or analogues; these are all bound in similar conformations. CMX, the analogue bound here, is present in a conformation most like that observed for CoA in *Pf*CS (Figure 5). Residues from a single monomer form hydrogen bonds with CMX, with the exception being Arg414 (*Pf*CS Arg353) from the adjacent monomer. Other residues whose side chains form hydrogen bonds with CMX include (*Pf*CS numbering in parentheses) His272 (His223), Lys307 (Lys256), Arg314 (Arg263), Arg364 (Lys305), Asn369 (Asn310), and Asp371 (Asp312); residues with main chain atoms forming hydrogen bonds with CMX include Ala271 (Ile222), Leu308 (Ile257), Gly310 (Gly259), and Phe311 (Ala260). A water molecule forming a hydrogen bond to N3 of the CoA adenine moiety in *Pf*CS is replaced in *Aa*CS with the hydroxyl oxygen of Tyr360. This residue is located on a loop of the protein which is longer and differently oriented in *Aa*CS.

OAA and the carboxylate end of CMX are bound in an arrangement nearly identical to that observed in the *Gg*CS·OAA·CMX complex (*73*). This arrangement is consistent with the proposed mechanism (*64*, *74*) in which Asp375 abstracts a proton from the methyl group of acetyl-CoA, His274 stabilizes the negative charge on the resulting enolate anion, and His320 polarizes the OAA ketone, priming it for nucleophilic attack. The corresponding residues in *Aa*CS are Asp371, His272, and His313, respectively. Other residues forming hydrogen bonds with OAA in *Aa*CS are (*Gg*CS numbering in parentheses) His237 (His238), Asn240 (Asn242), Arg322 (Arg329), Arg396 (Arg401), and Arg417′ (Arg421′), where the prime indicates a residue from the adjacent monomer.

Type I CS crystal structures have been determined in both a closed form, in which AcCoA analogues, OAA, or products are bound, and an open, unliganded form. The only crystal structures available for type II CS enzymes are those for *Ec*CS in the open form. The open form of *Ec*CS differs from

Table 4: Comparison of Type II CS Crystal Structures

	*Aa*CS·OAA·CMX (2h12)	*Ec*CS·NADH (1nxg)
size		
length (no. of amino acids)	436	427
polar accessible surface area (%)	51	49
hexamer volume (Å^3)	458200	475900
no. of cavities/volume (Å^3)	59/257	97/887
no. of hydrogen bonds[a]		
intrasubunit (total/involving side chains)	381/133	339/110
intersubunit (total/involving side chains)	19/39	22/39
no. of salt bridges[a]		
intrasubunit	10	8
intersubunit	3	1
% involving Arg	92	78
composition		
% Arg	5.0	5.6
% Cys	0.9	1.6
% Ser	4.6	5.9
% Thr	5.3	6.6
% Tyr	3.9	3.7
% Ile and Val	12.1	11.3
% Asp and Glu	9.8	12.4
% Arg and Lys	10.6	11.0
acidic and basic surface residues[a]		
no. of Arg residues (charge-compensated/not compensated)[b]	10/11	6/17
no. of Lys residues (charge-compensated/not compensated)[b]	2/20	2/21
no. of Asp residues (charge-compensated/not compensated)[c]	5/13	5/20
no. of Glu residues (charge-compensated/not compensated)[c]	8/12	2/24

[a] Per subunit. [b] Charge-compensated is defined as forming a side chain hydrogen bond with Asp or Glu. [c] Charge-compensated is defined as forming a side chain hydrogen bond with Arg or Lys.

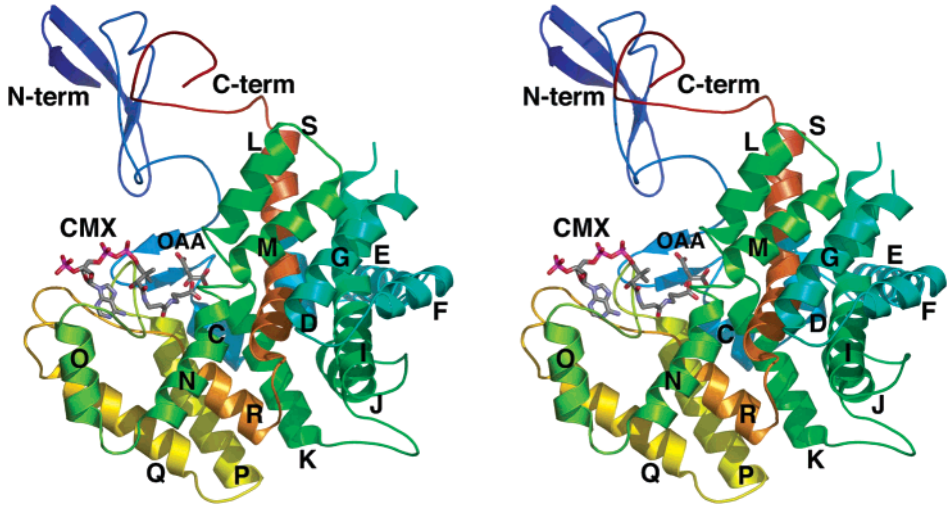

FIGURE 4: Divergent stereodiagram Ribbons rendering of the *Aa*CS·OAA·CMX monomer structure, with ligands illustrated as sticks. Helices are labeled according to the *Gg*CS convention (*4*). Residues are colored from the N-terminus (blue) to the C-terminus (red).

the open form of type I enzymes. In particular, two helices comprising *Ec*CS residues 261−302 (*Gg*CS residues 271−317) are translated outward from the interior of the protein. This rotation can be visualized as resulting from a rotation about the Gly262 Cα−C bond. Given these conformational differences between type I and type II enzymes in the open form, one might predict that the closed forms would differ as well. However, *Aa*CS complexed with OAA and CMX is in the closed form with a structure very similar to the closed form of the type I CS enzymes (rmsd of 1.47 Å over 331 residues).

Although the relative orientation of the three dimers is the same in the open *Ec*CS structures and the closed *Aa*CS structure, several localized differences exist (Supporting Information, Figure S14). Relative to the *Ec*CS structure, *Aa*CS has helix N moved inward (toward the CMX binding site), helix O moved up (toward the N-termini) and slightly outward, and helix Q with its following turn moved upward. The C-termini are in different locations.

To determine whether the open form of *Aa*CS resembles that of *Ec*CS, we attempted to crystallize *Aa*CS in the absence of substrates or inhibitors. No crystals of unliganded

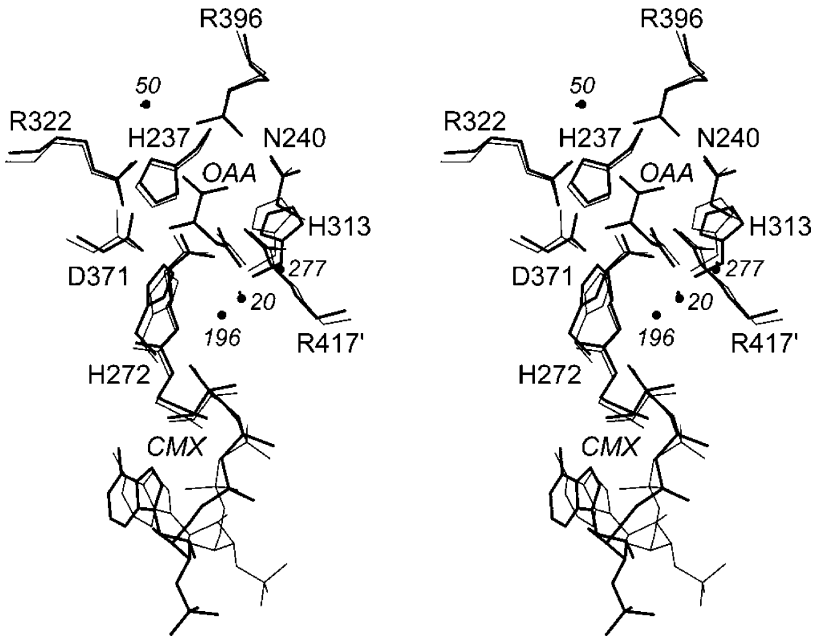

FIGURE 5: Divergent stereodiagram of the active site region. Ligands and key active site residues in the *Aa*CS·OAA·CMX structure (thick lines, PDB entry 2h12) are superimposed on the analogous components of the *Gg*CS·OAA·CMX structure (thin lines, PDB entry 1csi). The residue numbering is for *Aa*CS, with *Gg*CS numbering in parentheses: H237 (H238), N240 (N242), H272 (H274), H313 (H320), D371 (D375), R322 (R329), R396 (R401), and R417′ (R421′). Water numbers are given in small italic digits.

enzyme formed under the conditions used for the complex. Like *Aa*CSH6, unliganded *Aa*CS^{intein} formed small, poorly diffracting crystals from a variety of PEG precipitants. *Aa*CS^{intein} crystals grown under conditions similar to those reported for *Ec*CS [2 M ammonium sulfate, 4−5% (v/v) PEG400, and 100 mM HEPES (pH 7.5)] had better morphology but were very sensitive to handling and yielded only an incomplete data set with usable signal to ~6 Å; this crystal displayed partial hemihedral twinning with a twinning fraction of 0.3. Structure determination using this poor-quality data set was not pursued.

Two structures of type II *Ec*CS bound to NADH are available (PDB entries 1nxg and 1owb). Although *Aa*CS is insensitive to allosteric inhibition by NADH, the structure of the vestigial NADH binding pocket is remarkably similar to that observed in the *Ec*CS·NADH complexes. Several NADH-contacting residues that are conserved among NADH-sensitive CSs (*9*) are found in similar orientations in *Aa*CS (*Ec*CS numbering in parentheses): Thr119 (Thr111), His122 (His114), Arg171 (Arg163), Lys175 (Lys167), Gly189 (Gly181), Pro195 (Pro187), Asn197 (Asn189), and Glu215 (Glu207). In the *Aa*CS crystal structure, a sulfate ion is bound in a position occupied by the NADH β-phosphate (nicotinamide side) in the *Ec*CS·NADH complexes. This sulfate ion forms hydrogen bonds with His118 (His110), Tyr153 (Tyr145), Arg171, and Lys175.

Several structural differences are apparent in this region (Figure 6). *Ec*CS Met112, implicated as being key for NADH binding (*9*), is replaced with Leu120 in *Aa*CS; however, this is a conservative mutation, and the side chain conformations are similar. Thr204 is replaced in *Aa*CS with Arg212, the side chain of which could presumably block NADH binding. A possible compensatory change is found on the opposite side of the binding pocket, where *Ec*CS Arg109 is replaced with Asn. The guanidinium groups of *Aa*CS Arg212 and

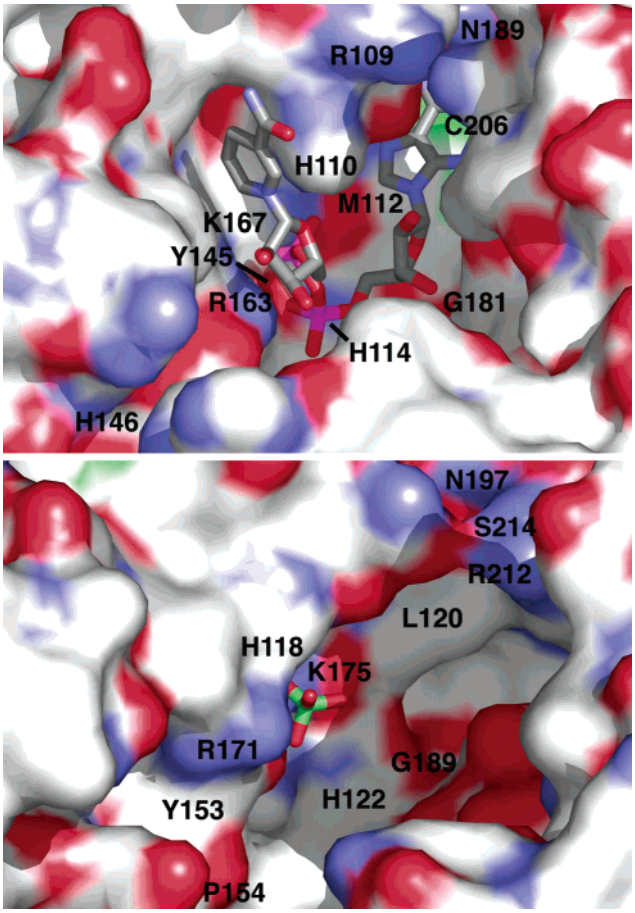

FIGURE 6: Surface rendering of the NADH binding pocket in the *Ec*CS·NADH complex (top, PDB entry 1nxg) and the analogous region in the *Aa*CS·OAA·CMX complex (bottom, PDB entry 2h12). Surfaces are colored by atom type: white for carbon, blue for nitrogen, red for oxygen, and green for sulfur. Bound NADH and sulfate are shown as stick renderings.

*Ec*CS Arg109 occupy the same region over the NADH adenine ring. Perhaps more important, the side chain of *Aa*CS His118 (*Ec*CS His110), which forms a bridge between the two halves of the horseshoe-shaped NADH, is shifted in *Aa*CS with respect to its position in both NADH-bound and unliganded *Ec*CS. Also, *Ec*CS His146 is replaced with *Aa*CS Pro154, and residues following this Pro constitute a disordered loop in the *Aa*CS crystal structure. This substitution may prevent the loop joining helices G and I from properly folding to form a binding pocket for the nicotinamide end of NADH. Soaking *Aa*CS crystals in 1 mM NADH did not result in additional electron density in the region corresponding to the *Ec*CS NADH binding site.

DISCUSSION

The cytoplasmic pH of *A. aceti* decreases with external pH over a wide range, due to the influx of acetic acid. In contrast, the cytoplasm of most terrestrial acidophiles, acid-resistant bacteria, and alkaliphiles are protected from environmental stresses by impermeable membranes, cytoplasmic buffering agents, and other barrier strategies (*14*). Proteins from these organisms are therefore not necessarily more resistant to environmental stresses than are their "neutralophile" analogues. In contrast, *A. aceti* proteins are forced to adapt to continuous exposure to acetic acid at low pH. To better understand the mechanisms of acid resistance in *A. aceti* and to explore how its enzymes function in acidic environments, we have biochemically characterized *Aa*CS, showing that it is resistant to acid-mediated inactivation and determining its structure in a catalytically competent state.

There are at least three nonexclusive ways for *Aa*CS to remain active at low pH: it might be optimized for catalytic function at low pH, it might have improved stability at low pH, or it might be protected by chaperone proteins. There is no evidence that *Aa*CS has been optimized to have higher activity at low pH; *Aa*CS is active over a broad pH range with well-separated pK_a values, like other CS forms (*31*). The K_m and K_d values for OAA are similar and relatively constant (within a factor of 2) from neutral to low pH (Table 1; Supporting Information, Figure S8), indicating that formation of the *Aa*CS·OAA complex would not be particularly inhibited by low pH. Mechanistic investigations of *Aa*CS have thus far not revealed any major alterations in proton transfers (H. Jiang and T. J. Kappock, unpublished observations). In addition, the sequence and structure of *Aa*CS show conservation of all key active site residues (Supporting Information, Figure S15). When bound to OAA and CMX, *Aa*CS adopts the same closed structure observed for type I CS enzymes. Both OAA and the AcCoA analogue bind in the same conformations as in the other CS structures. This lack of optimization for activity at low pH is not surprising, as the cytoplasmic pH range tolerated by *A. aceti* is both unusually acidic and unusually broad (*13*). Retaining some activity over a broad pH range is likely to be more important than optimizing specific activity for a particular pH.

In contrast, several lines of evidence indicate that *Aa*CS is resistant to acid-mediated inactivation during prolonged incubations at low pH. Thermal unfolding assessed by CD showed substantial stabilization of *Aa*CS at low pH relative to a PCS control, indicating that the folded state of *Aa*CS is stable over a broad pH range. *Aa*CS was quite resistant to inactivation at moderately acidic pH, with half-lives of hours to days in an assay that monitored residual activity as a reporter for folded protein. Inactivation rates sharply increase only as the pH approaches 3.5, the lower limit of the known cytoplasmic pH for *A. aceti* (*13*), showing that *Aa*CS is durable under all physiologically relevant conditions. Since these studies were performed with pure *Aa*CS, chaperones are not needed to explain the observed stability. There is also no evidence that citrate, the product of *Aa*CS and a potent Hofmeister (*75*) "salting-out" (stabilizing) anion (*76*), has any role in regulating *Aa*CS activity or stabilizing *A. aceti* proteins. The observed ~5 fold acceleration of *Aa*CS inactivation in citrate versus phosphate buffer at pH 3.5 suggests citrate exerts a different anion-specific effect on *Aa*CS (*77*). Both acetate and citrate, each of which might accumulate in the *A. aceti* cytoplasm, were only moderate reversible inhibitors of *Aa*CS, although citrate was a more potent inhibitor at pH 4 (Supporting Information, Figure S2 and Table S4). A similar resistance to acid without catalytic retooling for low-pH optima is observed for *A. aceti* alanine racemase (*78*) and PurE (*79*).

Many different factors contribute to the stability of a protein; some of these factors may provide stability under a variety of conditions, while others allow the protein to remain stable under a specific condition such as high temperature or low pH. Structural features that stabilize a folded protein structure in general include a well-packed hydrophobic core, a lack of electrostatic repulsion, and hydrogen bonding to compensate for removal of polar or charged groups from aqueous solution. Some specific features thought to contribute to thermostability include short sequence length (*80*) and deletion of exposed loops (*81*), formation of ion pairs (*82*), a preference for Arg and Tyr residues and avoidance of Cys and Thr residues (*83*), a preference for charged residues and for β-branched hydrophobic residues (*80*), and a patchwork of oppositely charged surface residues (*84*).

While some of these specific features may contribute to acid stability as well, others may be ineffective or even deleterious at low pH. For example, formation of ion pairs within a protein may be advantageous only at elevated temperatures, where the energy penalty for desolvation of the side chains is smaller (*85*). Similarly, surface acidic residues no longer repel each other low pH, possibly promoting protein aggregation. Specific characteristics thought to improve acid stability include reduced surface charge density to prevent electrostatic repulsion at pHs above and below the pK_as of acidic surface residues (*86*), an infrequent overall occurrence of charged residues and particularly basic residues (*86*−*88*), a frequent occurrence of the polar neutral residues Ser and Thr (*86*), and oligomer formation to reduce exposed surface area (*89*).

Surprisingly, when compared to *Ec*CS, *Aa*CS lacks many of the anticipated characteristics of an acid-stable protein (Table 4). While *Aa*CS has a moderately reduced proportion of charged residues (20.6% vs 23.4% in *Ec*CS), the differences in surface charge are most striking. Rather than avoiding positive charge on the surface, *Aa*CS has a surface abundantly decorated with basic side chains (Figure 3). Compared with *Ec*CS, *Aa*CS also has many fewer uncompensated acidic residues on its surface (Table 4). This arrangement is likely more stable in the variable pH of the *A. aceti* cytoplasm (the pH falls from near-neutral to acidic

as saturating cell density is reached): a basic protein surface will undergo less charge fluctuation as the cytoplasmic pH varies. In contrast, an acidic protein would have an altered charge decoration and may experience a charge inversion, each of which could destabilize a folded protein. A positively charged surface may also prevent penetration of the surface by hydronium ions at low pH.

Despite adaptations that render *Aa*CS acid-resistant, all key citrate synthase active site residues are conserved. *Aa*CS contains all of the active site arginines at positions 314, 322, 364, 396, 414 (Lys404 in *Ec*CS), and 417; this is not surprising because all are highly conserved residues, but it is striking because a buried cluster of basic residues would be expected to electrostatically destabilize acid-resistant proteins. When bound to OAA and CMX, *Aa*CS adopts the same closed structure observed for type I CS enzymes. Both OAA and the AcCoA analogue bind in the same conformations as in the other CS structures.

Some type II CS forms have added regulatory features, notably a strong NADH-mediated inhibition first observed with *Ec*CS (*3*). NADH inhibition allows facultative anaerobes to downregulate the citric acid cycle when growing anaerobically. *Aa*CS is only affected by NADH at nonphysiological concentrations in the mid-millimolar range. This observation is consistent with an analysis of NADH binding residues (*9*) and with subtle structural differences between the *Ec*CS NADH binding site and the vestigial site in *Aa*CS described above. Given the importance of *Aa*CS in acetic acid resistance, regulation by NADH might be deleterious.

ACKNOWLEDGMENT

We thank S. Spiess and P. Khayyat for technical assistance. We thank D. M. Hambly and J. B. Sperry for mass spectrometry expertise. We thank D. G. Drueckhammer for sharing unpublished synthetic procedures. We thank E. Strauss for the CoaD and CoaE plasmids. We thank M. Riley for help with preliminary fluorescence experiments and the CoaD and CoaE activity assays. We thank L. C. Kurz and G. R. Drysdale for advice and the gift of CitCoA. We thank A. M. Holtzer, M. Emerson Holtzer, L. C. Kurz, and J. Schaefer for the use of equipment. We thank J. Nix, C. Nelson, and Z. Chen for assistance with crystal screening, and data collection and processing. We thank T. J. Dolinsky and N. A. Baker for help with data analysis. We thank an anonymous reviewer for helpful comments.

SUPPORTING INFORMATION AVAILABLE

Materials, analytical procedures, synthesis of dethia-AcCoA and CMX, purification of $Aa\text{CS}^{dye}$ and *Aa*CSH6, thiol determinations, determinations of extinction coefficients, determination of OAA decomposition rates and binding constants, and evaluation of alternative substrates and inhibitors (four tables and 15 figures). This material is available free of charge via the Internet at http://pubs.acs.org.

REFERENCES

1. Remington, S. J. (1992) Structure and mechanism of citrate synthase, *Curr. Top. Cell. Regul. 33*, 209−229.
2. Nguyen, N. T., Maurus, R., Stokell, D. J., Ayed, A., Duckworth, H. W., and Brayer, G. D. (2001) Comparative analysis of folding and substrate binding sites between regulated hexameric type II citrate synthases and unregulated dimeric type I enzymes, *Biochemistry 40*, 13177−13187.
3. Weitzman, P. D. J. (1966) Regulation of citrate synthase activity in *Escherichia coli*, *Biochim. Biophys. Acta 128*, 213−215.
4. Remington, S., Wiegand, G., and Huber, R. (1982) Crystallographic refinement and atomic models of two different forms of citrate synthase at 2.7 and 1.7 Å resolution, *J. Mol. Biol. 158*, 111−152.
5. Wiegand, G., Remington, S., Deisenhofer, J., and Huber, R. (1984) Crystal structure analysis and molecular model of a complex of citrate synthase with oxaloacetate and S-acetonyl-coenzyme A, *J. Mol. Biol. 174*, 205−219.
6. Wiegand, G., and Remington, S. J. (1986) Citrate synthase: Structure, control, and mechanism, *Annu. Rev. Biophys. Biophys. Chem. 15*, 97−117.
7. Russell, R. J. M., Ferguson, J. M. C., Hough, D. W., Danson, M. J., and Taylor, G. L. (1997) The crystal structure of citrate synthase from the hyperthermophilic archaeon *Pyrococcus furiosus* at 1.9 Å resolution, *Biochemistry 36*, 9983−9994.
8. Russell, R. J. M., Gerike, U., Danson, M. J., Hough, D. W., and Taylor, G. L. (1998) Structural adaptations of the cold-active citrate synthase from an Antarctic bacterium, *Structure 6*, 351−361.
9. Maurus, R., Nguyen, N. T., Stokell, D. J., Ayed, A., Hultin, P. G., Duckworth, H. W., and Brayer, G. D. (2003) Insights into the evolution of allosteric properties. The NADH binding site of hexameric type II citrate synthases, *Biochemistry 42*, 5555−5565.
10. Stokell, D. J., Donald, L. J., Maurus, R., Nguyen, N. T., Sadler, G., Choudhary, K., Hultin, P. G., Brayer, G. D., and Duckworth, H. W. (2003) Probing the roles of key residues in the unique regulatory NADH binding site of type II citrate synthase of *E. coli*, *J. Biol. Chem. 278*, 35435−35443.
11. Fukaya, M., Takemura, H., Okumura, H., Kawamura, Y., Horinouchi, S., and Beppu, T. (1990) Cloning of genes responsible for acetic acid resistance in *Acetobacter aceti*, *J. Bacteriol. 172*, 2096−2104.
12. Asai, T. (1968) *Acetic acid bacteria. Classification and biochemical activities*, University of Tokyo Press, Tokyo, Japan.
13. Menzel, U., and Gottschalk, G. (1985) The internal pH of *Acetobacterium wieringae* and *Acetobacter aceti* during growth and production of acetic acid, *Arch. Microbiol. 143*, 47−51.
14. Booth, I. R. (1985) Regulation of cytoplasmic pH in bacteria, *Microbiol. Rev. 49*, 359−378.
15. Greenfield, S., and Claus, G. W. (1972) Nonfunctional tricarboxylic acid cycle and the mechanism of glutamate biosynthesis in *Acetobacter suboxydans*, *J. Bacteriol. 112*, 1295−1301.
16. Macauley, S., McNeil, B., and Harvey, L. M. (2001) The genus *Gluconobacter* and its applications in biotechnology, *Crit. Rev. Biotechnol. 21*, 1−25.
17. Prust, C., Hoffmeister, M., Liesegang, H., Wiezer, A., Fricke, W. F., Ehrenreich, A., Gottschalk, G., and Deppenmeier, U. (2005) Complete genome sequence of the acetic acid bacterium *Gluconobacter oxydans*, *Nat. Biotechnol. 23*, 195−200.
18. Rius, N., Francia, A., Solé, M., and Lorén, J. G. (1995) Buffering capacity and membrane H^+ conductance of acetic acid bacteria, *J. Ind. Microbiol. 14*, 17−20.
19. Mesa, M. M., Caro, I., and Cantero, D. (1996) Viability reduction of *Acetobacter aceti* due to the absence of oxygen in submerged cultures, *Biotechnol. Prog. 12*, 709−712.
20. Muraoka, H., Watabe, Y., and Ogasawara, N. (1982) Effect of oxygen deficiency on acid production and morphology of bacterial cells in submerged acetic fermentation by *Acetobacter aceti*, *J. Ferment. Technol. 60*, 171−180.
21. Nakano, S., Fukaya, M., and Horinouchi, S. (2004) Enhanced expression of aconitase raises acetic acid resistance in *Acetobacter aceti*, *FEMS Microbiol. Lett. 235*, 315−322.
22. Duckworth, H. W., and Tong, E. K. (1976) The binding of reduced nicotinamide adenine dinucleotide to citrate synthase of *Escherichia coli* K12, *Biochemistry 15*, 108−114.
23. de Lemos Esteves, F., Ruelle, V., Lamotte-Brasseur, J., Quinting, B., and Frère, J.-M. (2004) Acidophilic adaptation of family 11 endo-β-1,4-xylanases: Modeling and mutational analysis, *Protein Sci. 13*, 1209−1218.
24. Martin, D. P., Bibart, R. T., and Drueckhammer, D. G. (1994) Synthesis of novel analogs of acetyl coenzyme A: Mimics of enzyme reaction intermediates, *J. Am. Chem. Soc. 116*, 4660−4668.
25. Xun, J. (2002) Ph.D. Thesis, State University of New York, Stony Brook, NY.

26. Herbert, A. A., and Guest, J. R. (1968) Biochemical and genetic studies with lysine+methionine mutants of *Escherichia coli*: Lipoic acid and α-ketoglutarate dehydrogenase-less mutants, *J. Gen. Microbiol. 53*, 363−381.
27. Reissig, J. L., and Wollman, E. L. (1963) Transduction of galactose markers by tempered bacteriophages 82 and 434 of *Escherichia coli*, *Ann. Inst. Pasteur 105*, 774−779.
28. Unger, K. (1984) High-performance size-exclusion chromatography, *Methods Enzymol. 104*, 154−169.
29. Srere, P. A., Brazil, H., and Gonen, L. (1963) Citrate condensing enzyme of pigeon breast muscle and moth flight muscle, *Acta Chem. Scand. 17*, S129−S134.
30. Srere, P. A. (1969) Citrate synthase, *Methods Enzymol. 13*, 3−11.
31. Kosicki, G. W., and Srere, P. A. (1961) Kinetic studies on the citrate-condensing enzyme, *J. Biol. Chem. 236*, 2560−2565.
32. Pflugrath, J. W. (1999) The finer things in X-ray diffraction data collection, *Acta Crystallogr. D55*, 1718−1725.
33. French, G. S., and Wilson, K. S. (1978) On the treatment of negative intensity observations, *Acta Crystallogr. A34*, 517−525.
34. Collaborative Computational Project Number 4 (1994) The CCP4 suite: Programs for protein crystallography, *Acta Crystallogr. D50*, 760−770.
35. Kleywegt, G. J., and Jones, T. A. (1996) Making the most of your search model, *CCP4/ESF-EACBM Newsletter on Protein Crystallography 32*, 32−36.
36. Vagin, A., and Teplyakov, A. (1997) MOLREP: An automated program for molecular replacement, *J. Appl. Crystallogr. 30*, 1022−1025.
37. Brünger, A. T., Adams, P. D., Clore, G. M., DeLano, W. L., Gros, P., Grosse-Kunstleve, R. W., Jiang, J.-S., Kuszewski, J., Nilges, M., Pannu, N. S., Read, R. J., Rice, L. M., Simonson, T., and Warren, G. L. (1998) Crystallography & NMR system: A new software suite for macromolecular structure determination, *Acta Crystallogr. D54*, 905−921.
38. Jones, T. A., Zou, J. Y., Cowan, S. W., and Kjeldgaard, M. (1991) Improved methods for building protein models in electron density maps and the location of errors in these models, *Acta Crystallogr. A47* (Part 2), 110−119.
39. Vagin, A. A., Steiner, R. A., Lebedev, A. A., Potterton, L., McNicholas, S., Long, F., and Murshudov, G. N. (2004) REFMAC5 dictionary: Organization of prior chemical knowledge and guidelines for its use, *Acta Crystallogr. D60*, 2184−2195.
40. Kleywegt, G. J., and Jones, T. A. (1997) Detecting folding motifs and similarities in protein structures, *Methods Enzymol. 277*, 525−545.
41. Pettersen, E. F., Goddard, T. D., Huang, C. C., Couch, G. S., Greenblatt, D. M., Meng, E. C., and Ferrin, T. E. (2004) UCSF chimera: A visualization system for exploratory research and analysis, *J. Comput. Chem. 25*, 1605−1612.
42. DeLano, W. L. (2002) *The PyMOL Users Manual*, DeLano Scientific, San Carlos, CA.
43. Kraulis, P. J. (1991) Molscript: A program to produce both detailed and schematic plots of protein structures, *J. Appl. Crystallogr. 24*, 946−950.
44. Merritt, E. A., and Bacon, D. J. (1997) Raster3D: Photorealistic molecular graphics, *Methods Enzymol. 277*, 505−524.
45. Dolinsky, T. J., Nielsen, J. E., McCammon, J. A., and Baker, N. A. (2004) PDB2PQR: An automated pipeline for the setup of Poisson-Boltzmann electrostatics calculations, *Nucleic Acids Res. 32*, W665−W667.
46. Baker, N. A., Sept, D., Joseph, S., Holst, M. J., and McCammon, J. A. (2001) Electrostatics of nanosystems: Application to microtubules and the ribosome, *Proc. Natl. Acad. Sci. U.S.A. 98*, 10037−10041.
47. Weitzman, P. D., and Ridley, J. (1983) Affinity chromatography of acyl-CoA utilizing enzymes on Procion Red-agarose, *Biochem. Biophys. Res. Commun. 112*, 1021−1026.
48. Schnier, P. D., Price, W. D., Jockusch, R. A., and Williams, E. R. (1996) Blackbody infrared radiative dissociation of bradykinin and its analogues: Energetics, dynamics, and evidence for salt-bridge structures in the gas phase, *J. Am. Chem. Soc. 118*, 7178−7189.
49. Gehrig, P. M., Hunziker, P. E., Zahariev, S., and Pongor, S. (2004) Fragmentation pathways of N^G-methylated and unmodified arginine residues in peptides studied by ESI-MS/MS and MALDI-MS, *J. Am. Soc. Mass Spectrom 15*, 142−149.
50. Ayed, A., Krutchinsky, A. N., Ens, W., Standing, K. G., and Duckworth, H. W. (1998) Quantitative evaluation of protein-protein and ligand-protein equilibria of a large allosteric enzyme by electrospray ionization time-of-flight mass spectrometry, *Rapid Commun. Mass Spectrom. 12*, 339−344.
51. Tong, E. K., and Duckworth, H. W. (1975) The quaternary structure of citrate synthase from *Escherichia coli* K12, *Biochemistry 14*, 235−241.
52. Sievers, M., Stöckli, M., and Teuber, M. (1997) Purification and properties of citrate synthase from *Acetobacter europaeus*, *FEMS Microbiol. Lett. 146*, 53−58.
53. Kurz, L. C., Shah, S., Frieden, C., Nakra, T., Stein, R. E., Drysdale, G. R., Evans, C. T., and Srere, P. A. (1995) Catalytic strategy of citrate synthase: Subunit interactions revealed as a consequence of a single amino acid change in the oxaloacetate binding site, *Biochemistry 34*, 13278−13288.
54. Weitzman, P. D. J. (1966) Reduced nicotinamide adenine dinucleotide as an allosteric effector of citrate synthase activity in *Escherichia coli*, *Biochem. J. 101*, 44C−45C.
55. Anderson, D. H., and Duckworth, H. W. (1988) In vitro mutagenesis of *Escherichia coli* citrate synthase to clarify the locations of ligand binding sites, *J. Biol. Chem. 263*, 2163−2169.
56. Faloona, G. R., and Srere, P. A. (1969) *Escherichia coli* citrate synthase. Purification and the effect of potassium on some properties, *Biochemistry 8*, 4497−4503.
57. Kurz, L. C., Drysdale, G., Riley, M., Tomar, M. A., Chen, J., Russell, R. J. M., and Danson, M. J. (2000) Kinetics and mechanism of the citrate synthase from the thermophilic archaeon *Thermoplasma acidophilum*, *Biochemistry 39*, 2283−2296.
58. Kurz, L. C., Fite, B., Jean, J., Park, J., Erpelding, T., and Callis, P. (2005) Photophysics of tryptophan fluorescence: Link with the catalytic strategy of the citrate synthase from *Thermoplasma acidophilum*, *Biochemistry 44*, 1394−1413.
59. Srere, P. A., and Kosicki, G. W. (1961) The purification of citrate-condensing enzyme, *J. Biol. Chem. 236*, 2557−2559.
60. Tipton, K. F., and Dixon, H. B. (1979) Effects of pH on enzymes, *Methods Enzymol. 63*, 183−234.
61. Kurz, L. C., Drysdale, G. R., Riley, M. C., Evans, C. T., and Srere, P. A. (1992) Catalytic strategy of citrate synthase: Effects of amino acid changes in the acetyl-CoA binding site on transition-state analog inhibitor complexes, *Biochemistry 31*, 7908−7914.
62. Pereira, D. S., Donald, L. J., Hosfield, D. J., and Duckworth, H. W. (1994) Active site mutants of *Escherichia coli* citrate synthase. Effects of mutations on catalytic and allosteric properties, *J. Biol. Chem. 269*, 412−417.
63. Handford, P. A., Ner, S. S., Bloxham, D. P., and Wilton, D. C. (1988) Site-directed mutagenesis of citrate synthase: The role of the active-site aspartate in the binding of acetyl-CoA but not oxaloacetate, *Biochim. Biophys. Acta 953*, 232−240.
64. Karpusas, M., Branchaud, B., and Remington, S. J. (1990) Proposed mechanism for the condensation reaction of citrate synthase: 1.9-Å structure of the ternary complex with oxaloacetate and carboxymethyl coenzyme A, *Biochemistry 29*, 2213−2219.
65. Bayer, E., Bauer, B., and Eggerer, H. (1981) Evidence from inhibitor studies for conformational changes of citrate synthase, *Eur. J. Biochem. 120*, 155−160.
66. Kurz, L. C., Nakra, T., Stein, R., Plungkhen, W., Riley, M., Hsu, F., and Drysdale, G. R. (1998) Effects of changes in three catalytic residues on the relative stabilities of some of the intermediates and transition states in the citrate synthase reaction, *Biochemistry 37*, 9724−9737.
67. Cantor, C. R., and Schimmel, P. R. (1980) *Techniques for the study of biological structure and function*, W. H. Freeman, San Francisco.
68. Srere, P. A. (1966) Citrate-condensing enzyme-oxalacetate binary complex. Studies on its physical and chemical properties, *J. Biol. Chem. 241*, 2157−2165.
69. Wieland, O., Weiss, L., and Eger-Neufeldt, I. (1964) Inhibition of enzymic citrate synthase by long-chain acylthioesters of coenzyme A, *Biochem. Z. 339*, 501−513.
70. Zhi, W., Srere, P. A., and Evans, C. T. (1991) Conformational stability of pig citrate synthase and some active-site mutants, *Biochemistry 30*, 9281−9286.
71. Ayed, A., and Duckworth, H. W. (1999) A stable intermediate in the equilibrium unfolding of *Escherichia coli* citrate synthase, *Protein Sci. 8*, 1116−1126.
72. Settembre, E. C., Chittuluru, J. R., Mill, C. P., Kappock, T. J., and Ealick, S. E. (2004) Acidophilic adaptations in the structure of *Acetobacter aceti* N^5-carboxyaminoimidazole ribonucleotide mutase (PurE), *Acta Crystallogr. D60*, 1753−1760.
73. Usher, K. C., Remington, S. J., Martin, D. P., and Drueckhammer, D. G. (1994) A very short hydrogen bond provides only moderate

stabilization of an enzyme-inhibitor complex of citrate synthase, *Biochemistry 33*, 7753−7759.
74. Evans, C. T., Kurz, L. C., Remington, S. J., and Srere, P. A. (1996) Active site mutants of pig citrate synthase: Effects of mutations on the enzyme catalytic and structural properties, *Biochemistry 35*, 10661−10672.
75. Hofmeister, F. (1888) Zur Lehre von der Wirkung der Salze. Zweite Mittheilung, *Arch. Exp. Pathol. Pharmakol. 24*, 249−260.
76. Kaushik, J. K., and Bhat, R. (1999) A mechanistic analysis of the increase in the thermal stability of proteins in aqueous carboxylic acid salt solutions, *Protein Sci. 8*, 222−233.
77. Arakawa, T., and Timasheff, S. N. (1984) Mechanism of protein salting in and salting out by divalent cation salts: Balance between hydration and salt binding, *Biochemistry 23*, 5912−5923.
78. Francois, J. A., and Kappock, T. J. (2006) Alanine racemase from the acidophile *Acetobacter aceti*, *Protein Expression Purif.* (in press).
79. Constantine, C. Z., Starks, C. M., Mill, C. P., Ransome, A. E., Karpowicz, S. J., Francois, J. A., Goodman, R. A., and Kappock, T. J. (2006) Biochemical and structural studies of N^5-carboxyaminoimidazole ribonucleotide mutase (PurE) from the acidophilic bacterium *Acetobacter aceti*, *Biochemistry 45*, 8193−8208.
80. Chakravarty, S., and Varadarajan, R. (2000) Elucidation of determinants of protein stability through genome sequence analysis, *FEBS Lett. 470*, 65−69.
81. Thompson, M. J., and Eisenberg, D. (1999) Transproteomic evidence of a loop-deletion mechanism for enhancing protein thermostability, *J. Mol. Biol. 290*, 595−604.
82. Li, W. T., Shriver, J. W., and Reeve, J. N. (2000) Mutational analysis of differences in thermostability between histones from mesophilic and hyperthermophilic archaea, *J. Bacteriol. 182*, 812−817.
83. Kumar, S., Tsai, C. J., and Nussinov, R. (2000) Factors enhancing protein thermostability, *Protein Eng. 13*, 179−191.
84. Strickler, S. S., Gribenko, A. V., Keiffer, T. R., Tomlinson, J., Reihle, T., Loladze, V. V., and Makhatadze, G. I. (2006) Protein stability and surface electrostatics: A charged relationship, *Biochemistry 45*, 2761−2766.
85. Elcock, A. H. (1998) The stability of salt bridges at high temperatures: Implications for hyperthermophilic proteins, *J. Mol. Biol. 284*, 489−502.
86. Schwermann, B., Pfau, K., Liliensiek, B., Schleyer, M., Fischer, T., and Bakker, E. P. (1994) Purification, properties and structural aspects of a thermoacidophilic α-amylase from *Alicyclobacillus acidocaldarius* ATCC 27009. Insight into acidostability of proteins, *Eur. J. Biochem. 226*, 981−991.
87. Goto, Y., and Nishikiori, S. (1991) Role of electrostatic repulsion in the acidic molten globule of cytochrome *c*, *J. Mol. Biol. 222*, 679−686.
88. Yang, A. S., and Honig, B. (1993) On the pH dependence of protein stability, *J. Mol. Biol. 231*, 459−474.
89. Ha, N.-C., Oh, S.-T., Sung, J. Y., Cha, K. A., Lee, M. H., and Oh, B.-H. (2001) Supramolecular assembly and acid resistance of *Helicobacter pylori* urease, *Nat. Struct. Biol. 8*, 505−509.

BI061083K